White Dwarfs as Dark Matter Detectors

Peter W. Graham,[1] Ryan Janish,[2] Vijay Narayan,[2] Surjeet Rajendran,[2] and Paul Riggins[2]

[1]*Stanford Institute for Theoretical Physics, Department of Physics, Stanford University, Stanford, CA, 94305*
[2]*Berkeley Center for Theoretical Physics, Department of Physics,*
University of California, Berkeley, CA 94720, USA

If dark matter (DM) is capable of sufficiently heating a local region in a white dwarf, it will trigger runaway fusion and ignite a type 1a supernova. This was originally proposed in [1] and used to constrain primordial black holes which transit and heat a white dwarf via dynamical friction. In this paper, we extend the analysis of white dwarf DM detection to candidates with non-gravitational interactions that heat through the production of standard model (SM) particles. We consider a general class of models in which DM-DM collisions, DM decays, or DM transits including a SM scattering interaction produce particles that subsequently deposit energy inside the star. The existence of long-lived white dwarfs and the observed supernovae rate provide constraints for such models. As a concrete example, we rule out supersymmetric Q-ball DM in a large region of parameter space fundamentally inaccessible to terrestrial detection. It is also intriguing that the DM-induced ignition discussed in this work provide an alternative mechanism of triggering supernovae from sub-Chandrasekhar Mass progenitors.

Contents

I. INTRODUCTION

Identifying the nature of dark matter (DM) remains one of the clearest paths beyond the Standard Model (SM) and it is thus fruitful to study the observable signatures of any yet-allowed candidate. Many terrestrial direct detection experiments are designed to search for DM, e.g. [2, 3], yet these lose sensitivity to heavier DM due to its diminished number density. Even for a strongly-interacting candidate, if the DM mass is above $\sim 10^{22}$ GeV a detector of size $\sim (100 \text{ m})^2$ will register fewer than one event per year. While these masses are large compared to those of fundamental particles, it is reasonable to suppose that DM may exist as composite states just as the SM produces complex structures with mass much larger than fundamental scales (e.g. you, dear reader). Currently there is a wide range of unexplored parameter space for DM candidates less than $\sim 10^{48}$ GeV, above which the DM will have observable gravitational microlensing effects [4]. For such ultra-heavy DM, indirect signatures in astrophysical systems are a natural way forward. One possibility proposed by [1] is that DM can trigger runaway fusion and ignite type 1a supernovae (SN) in sub-Chandrasekhar white dwarf (WD) stars. This is even more interesting in light of recent observations that an $\mathcal{O}(1)$ fraction of type 1a SN are due to sub-Chandrasekhar progenitors [5, 6]. While astrophysical mechanisms for these events have been proposed [7–9], the situation is yet unclear and it is an exciting possibility that these SN arise from DM interactions.

Runaway thermonuclear fusion requires both a heating event and the lack of significant cooling which might quench the process. The WD medium is particularly suited to this as it is dominated by degeneracy pressure and undergoes minimal thermal expansion, which is the mechanism that regulates fusion in main sequence stars. Thermal diffusion is the primary cooling process in a WD and it can be thwarted by heating a large enough region. The properties of a localized heating necessary to trigger runaway fusion were computed in [10]. Consequently, it was realized [1] that if DM is capable of sufficiently heating a WD in this manner, it will result in a SN with sub-Chandrasekhar mass progenitor. This was used to constrain primordial black holes which transit a WD and cause heating by dynamical friction, although the authors of [1] identify several other heating mechanisms which may be similarly constrained.

In this paper, we examine DM candidates with non-gravitational interactions that cause heating through the production of SM particles. An essential ingredient in this analysis is understanding the length scales over which SM particles deposit energy in a WD medium. We find that most high energy particles thermalize efficiently with ions in the star, nearly independent of species or initial energy. Particle production is thus an effective means of heating WDs. Constraints on these DM candidates come from either observing specific, long-lived WDs or by comparing the measured rate of type 1a SN with that expected due to DM. It is important to note that these constraints are complementary to direct searches—it is more massive DM that is likely to trigger SN, but also more massive DM that has low terrestrial flux. The WD detector excels in this regime due to its large surface area $\sim (10^4 \text{ km})^2$, long lifetime $\sim$ Gyr, and galactic abundance. We demonstrate these constraints for generic classes of DM models that produce SM particles via DM-DM collisions, DM decays, or DM transits including a SM scattering interaction. As a concrete example we consider ultra-heavy Q-ball DM as found in supersymmetric extensions of the SM.

The rest of the paper is organized as follows. We begin in Section II by reviewing the mechanism of runaway fusion in a WD. In Section III we study the non-gravitational heating of a WD due to the production of high-energy SM particles. Detailed calculations of the stopping of such particles are provided in Appendix A. In Section IV we parameterize the explosiveness and event rate for generic classes of DM-WD encounters, and in Section V we derive schematic constraints on such models. Finally we specialize to the case of Q-balls in Section VI, and conclude in Section VII.

II. WHITE DWARF RUNAWAY FUSION

We first review the conditions for which a local energy deposition in a WD results in runaway fusion. Any energy deposit will eventually heat ions within some localized region—parameterize this region by its linear size L_0, total kinetic energy $\mathcal{E}_0$ and typical temperature T_0. These scales evolve in time, but it will be useful to describe a given heating event by their initial values.

The fate of a heated region is either a nonviolent diffusion of the excess energy across the star, or a runaway fusion chain-reaction that destroys the star. The precise outcome depends on L_0, $\mathcal{E}_0$ and T_0. There is a critical temperature T_f, set by the energy required for ions to overcome their mutual Coulomb barrier, above which fusion occurs. For carbon burning, $T_f \sim$ MeV [11]. Any heated region $T_0 > T_f$ will initially support fusion, although this is not sufficient for runaway as cooling processes may rapidly lower the temperature below T_f. This cooling will not occur if the corresponding timescale is larger than the timescale at which fusion releases energy. Cooling in a WD is dominated by thermal diffusion, and the diffusion time increases as the size of the heated region. However, the timescale for heating due to fusion is independent of region size. Thus, for a region at temperature $\gtrsim T_f$, there is a critical size above which the heated region does not cool but instead initiates runaway. For a region at the critical fusion temperature
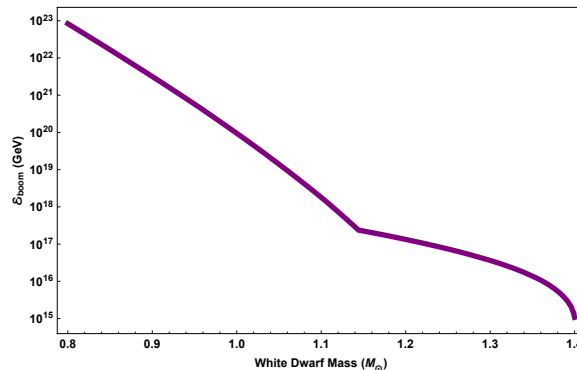
FIG. 1: The minimum energy deposit (2) necessary to trigger runaway fusion, based on numerical results for λ_T [10] and the WD mass-density relation [12]

.

T_f, we call this critical size the *trigger size* λ_T. The value of λ_T is highly dependent on density, and in a WD is set by the thermal diffusivity of either photons or degenerate electrons. This critical length scale has been computed numerically in [10] for a narrow range of WD densities and analytically scaled for other WD masses in [1]. As in [1], we will restrict our attention to carbon-oxygen WDs in the upper mass range $\sim 0.85 - 1.4\ M_\odot$ (these will yield the most stringent constraints on DM). This corresponds to a central number density of ions $n_{\mathrm{ion}} \sim 10^{30} - 10^{32}\ \mathrm{cm}^{-3}$ and a trigger size of $\lambda_T \sim 10^{-3} - 10^{-5}$ cm.

If a heated region is smaller than the trigger size, its thermal evolution is initially dominated by diffusion. However, this will still result in runaway fusion if the temperature is of order T_f by the time the region diffuses out to the trigger size. For our purposes it is more natural to phrase this in terms of the total energy $\mathcal{E}_0$ deposited during a heating event. Of course, the relation between energy $\mathcal{E}_0$ and temperature T_0 depends on the rate at which WD constituents—ions, electrons, and photons—thermalize with each other within the region size L_0. Given that the different species thermalize rapidly, the excess energy required to raise the temperature to T_f in a volume V is given by a sum of their heat capacities

$$\frac{\mathcal{E}_0}{V} \gtrsim \int_0^{T_f} dT (n_{\mathrm{ion}} + n_e^{2/3} T + T^3), \tag{1}$$

where n_e is the number density of electrons. Note that we use the heat capacity of a degenerate gas of electrons, since the Fermi energy $E_F \gtrsim \mathrm{MeV}$ for the densities we consider. The minimum energy deposit necessary to trigger runaway fusion is simply

$$\mathcal{E}_{\mathrm{boom}} \sim \lambda_T^3 (n_{\mathrm{ion}} T_f + n_e^{2/3} T_f^2 + T_f^4) \approx 10^{15} - 10^{23}\ \mathrm{GeV}. \tag{2}$$

$\mathcal{E}_{\mathrm{boom}}$ varies with λ_T over the range of WD densities and is plotted in Figure 1. Thus for a heating event characterized by its L_0, $\mathcal{E}_0$, and $T_0 \gtrsim T_f$, there is an *ignition condition*:

$$\mathcal{E}_0 \gtrsim \mathcal{E}_{\mathrm{boom}} \cdot \max\left\{1, \frac{L_0}{\lambda_T}\right\}^3. \tag{3}$$

Any $\mathcal{E}_0$ satisfying this condition is minimized for L_0 less than the trigger size, where it is also independent of the precise value of L_0. For broader deposits, the necessary energy is parametrically larger than $\mathcal{E}_{\mathrm{boom}}$ by a volume ratio $(L_0/\lambda_T)^3$. As a result, understanding the L_0 for different kinds of heating events in a WD is critical to determining whether or not they are capable of destroying the star.

III. PARTICLE HEATING OF WHITE DWARFS

We address now the possibility of DM heating the WD medium via the production of SM particles. The critical quantity is the length scale over which such SM particles heat the medium—this scale determines their efficiency in triggering runaway fusion as described by condition (3). Note that this is a question of purely SM physics. The unknown physics of DM will serve only to set the initial properties of the SM particles.
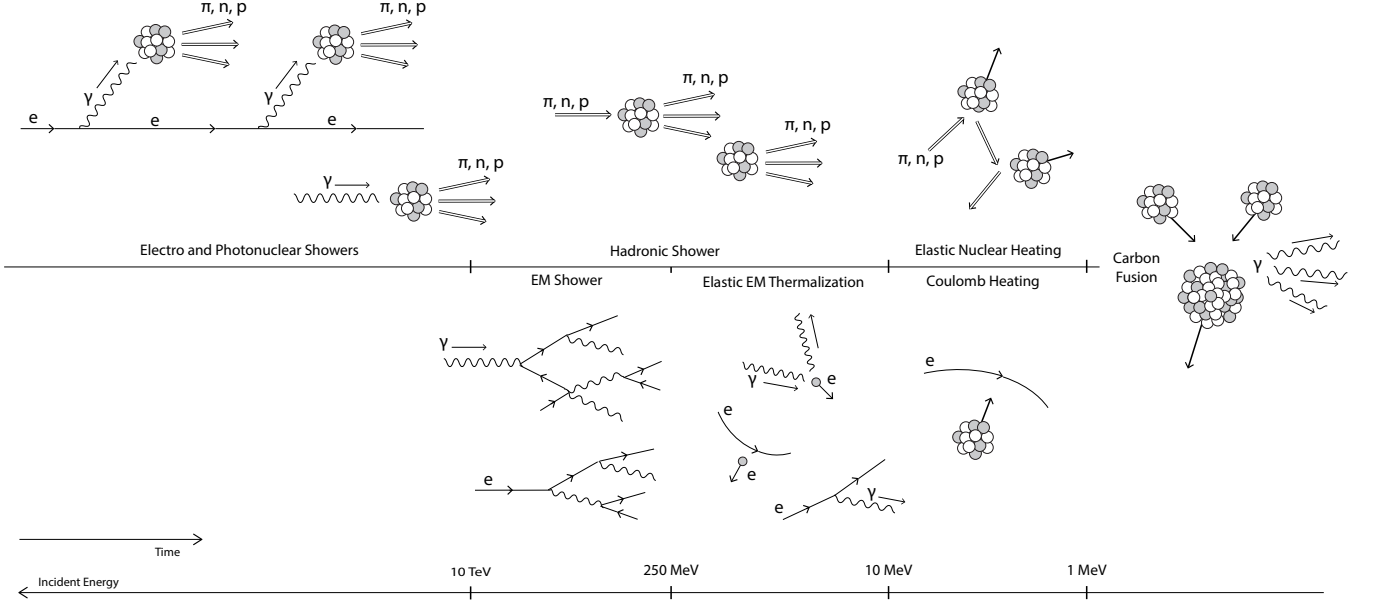
FIG. 2: Dominant energy loss and thermalization processes in the WD as a function of energy, with energy decreasing towards the right. Hadronic processes are shown in the upper panel and EM processes in the lower panel. High energy particles will induce showers that terminate into elastic thermalization of the WD ions, moving from left to right in the diagram.

One may have expected that efficient heating occurs only for a limited range of SM species and energies, thus restricting the set of DM candidates capable of producing SN. However, we find that SM particles tend to efficiently heat the WD regardless of species or energy—the length scale of heating is typically less than or of order the trigger size λ_T. This is accomplished primarily through hadronic showers initiated by collisions with carbon ions. In some cases electromagnetic showers are important, however at high energies these are suppressed by density effects and photons/electrons are dominated by hadronic interactions. These interactions rapidly stop high-energy particles due to the logarithmic nature of showers, transferring the energy into a cloud of low-energy particles which efficiently heat the WD medium through elastic scatters. In this light, the WD operates analogously to a particle detector, including hadronic and electromagnetic "calorimeter" components. Runaway fusion provides the necessary amplification to convert a detected event into a recordable signal, in this case a violent SN.

In the remainder of this section we present the above heating process in detail. A schematic for the flow of energy deposition is given in Figure **??**. We summarize the dominant source of energy loss and the resulting stopping lengths λ for SM particles of incident kinetic energy ϵ, approximated by

$$\lambda \sim \frac{\epsilon}{dE/dx}, \tag{4}$$

where dE/dx is the stopping power in the WD medium. These are plotted in Figures 4, **??**, 5, and **??**. A detailed treatment of the stopping powers is reserved for Appendix A. We will consider incident light hadrons, photons, electrons, and neutrinos—as we are concerned with triggering runaway fusion, we restrict our attention to energies $\epsilon \gg T_f \sim$ MeV.

A. High-Energy Showers

a. Hadronic Showers. Incident hadrons with kinetic energy larger than the nuclear binding scale ~ 10 MeV will undergo violent inelastic collisions with carbon ions resulting in an $\mathcal{O}(1)$ number of secondary hadrons. This results in a roughly collinear shower of hadrons of size

$$X_{\mathrm{had}} \sim \lambda_{\mathrm{inel}} \log\left(\frac{\epsilon}{10 \text{ MeV}}\right) \approx 10^{-6} \text{ cm} \left(\frac{10^{32} \text{ cm}^{-3}}{n_{\mathrm{ion}}}\right). \tag{5}$$

Here λ_{inel} is the mean free path for nuclear scatters, set by $\sigma_{\mathrm{inel}} \approx 100$ mb, and we have taken the logarithm to be ~ 10. The shower terminates into an exponential number of ~ 10 MeV hadrons with roughly equal fractions of pions,

protons, and neutrons. For a more detailed discussion of hadronic showers, see Appendix A B. Note that neutral pions of energy $10 - 100$ MeV have a decay length to photons of order $\delta_{\pi^0} \sim 10^{-6}$ cm. Hadronic showers will therefore generate an electromagnetic component carrying an $\mathcal{O}(1)$ fraction of the energy.

b. Photonuclear and Electronuclear Showers. The LPM effect (see next section) ensures that hadronic interactions become important at sufficiently high energies even for electrons and photons. A photons can interact hadronically via production of a quark-antiquark pair and directly induce a hadronic shower off ions. The only quantitative difference between these showers and purely hadronic ones is that they require a longer distance to initiate. Roughly, the photonuclear cross section is suppressed relative to the hadronic inelastic cross section by a factor of α, and so the photon range is

$$\lambda_{\gamma A} \sim \frac{\lambda_{\text{inel}}}{\alpha} \approx 10^{-5} \text{ cm} \left(\frac{10^{32} \text{ cm}^{-3}}{n_{\text{ion}}} \right). \tag{6}$$

Here $\lambda_{\gamma A}$ is the distance to initiate a hadronic shower, whereas the shower itself extends a distance X_{had}.

In the regime of strong LPM suppression, high-energy electrons also lose energy by inducing hadronic showers through virtual photons. This process is best described as a continuous energy loss of the electron into minimal ~ 10 MeV hadronic showers. The electronuclear stopping length is

$$\lambda_{eA} \approx 10^{-4} \text{ cm} \left(\frac{10^{32} \text{ cm}^{-3}}{n_{\text{ion}}} \right). \tag{7}$$

This is suppressed by an additional factor of α relative to the photonuclear interaction, although a full calculation also yields an $\mathcal{O}(10)$ logarithmic enhancement. We see that the electronuclear length scale λ_{eA} is at most larger than the trigger size by an order of magnitude.

c. Electromagnetic Showers. Of course, electrons and photons can also shower through successive bremsstrahlung and pair-production interactions. An electromagnetic shower proceeds until a critical energy ~ 100 MeV set by the scale at which these radiative processes become subdominant to Coulomb and Compton scattering. Below this scale radiation can still be important, though electromagnetic showers do not occur. Note that bremsstrahlung and pair-production are strictly forbidden for incident energies below the electron Fermi energy.

At sufficiently high electron/photon energies and nuclear target densities, electromagnetic showers are elongated due to the "Landau-Pomeranchuk-Migdal" (LPM) effect. High-energy radiative processes necessarily involve small momentum transfers to nuclei. These soft virtual photons cannot be exchanged with only a single ion, but rather interact simultaneously with multiple ions. This generates a decoherence, suppressing bremsstrahlung/pair-production above an energy E_{LPM} which scales inversely with density:

$$E_{\text{LPM}} \approx 1 \text{ MeV} \left(\frac{10^{32} \text{ cm}^{-3}}{n_{\text{ion}}} \right) \tag{8}$$

The corresponding shower lengths are

$$X_{\text{EM}} \approx X_0 \cdot \begin{cases} \left(\frac{\epsilon}{E_{\text{LPM}}} \right)^{1/2} & \epsilon > E_{\text{LPM}} \\ 1 & \epsilon < E_{\text{LPM}} \end{cases} \tag{9}$$

where

$$X_0 \approx 10^{-7} \text{ cm} \left(\frac{10^{32} \text{ cm}^{-3}}{n_{\text{ion}}} \right). \tag{10}$$

See Appendix A C for further details. At the highest WD densities radiative processes are always LPM-suppressed, while at lower densities we observe both regimes. In high-density WDs, electromagnetic showers completely carry the energy of $\sim 10^2 - 10^4$ MeV electrons and photons. The lower end of this range corresponds to the scale at which elastic scatters dominate, and the upper end corresponds to the scale at which photonuclear interactions dominate. In low-density WDs, the latter will occur at larger energy $\sim 10^6$ GeV. We emphasize that throughout the energy range where it is relevant, the length of an electromagnetic shower X_{EM} is never parametrically larger than the trigger size.

d. Neutrinos Neutrinos scatter off nuclei with a cross section that increases with energy. In these interactions, an $\mathcal{O}(1)$ fraction of the neutrino energy is transferred to the nucleus with the rest going to produced leptons—this is sufficient to start a hadronic shower [13, 14]. At an energy of $\sim 10^{11}$ GeV, [13] calculates the neutrino-nuclear cross section to be $\sim 10^{-32}$ cm^2. Conservatively assuming this value for even higher energies, we find a neutrino mean free path in a WD of order ~ 10 cm. While this distance is much too large to heat a WD via the release of multiple neutrinos, it is simply a displacement after which a compact shower of size X_{had} is initiated. As such, a *single* ultra-high energy neutrino released will heat the star just as high-energy hadrons do.
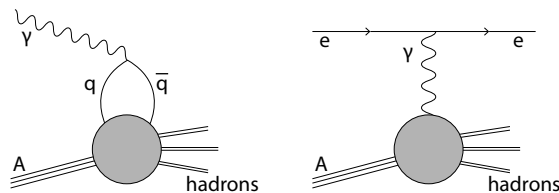
FIG. 3: Photonuclear (left) and Electronuclear (right) interactions. The shaded interaction contains, at high energies, the familiar point-like processes of deep inelastic nucleon scattering, while for energies below $\Lambda_{\rm QCD}$ is best described by exchange of virtual mesons.

B. Low-Energy Elastic Heating

The showers of high-energy particles described above terminate in a cloud of low-energy $\epsilon \sim 10$ MeV neutrons, protons, and charged pions, and $\epsilon \sim 10 - 100$ MeV electrons and photons. Of course, particles at these energies may also be directly produced by the DM. At these energies, elastic nuclear, Coulomb, and Compton scatters dominate and eventually lead to the thermalization of ions. The stopping powers for these processes are calculated in Appendix A B and A D.

a. *Nucleons and Pions.* Neutrons and neutral pions are the simplest species we consider, interacting at low-energies only through elastic nuclear scatters characterized by a cross section $\sigma_{\rm el} \approx$ b. Note that the mass hierarchy between these particles and the ions requires $\sim 10 - 100$ scatters to transfer the hadron's energy in the form of a random-walk. This elastic heating range is approximately

$$\lambda_{\rm el} \approx 10^{-7} \text{ cm} \left(\frac{10^{32} \text{ cm}^{-3}}{n_{\rm ion}} \right), \tag{11}$$

and is always less than the trigger size. Note that this may or may not be shorter than the neutral pion decay length δ_{π^0}, depending on the WD density. Low-energy neutrons thus always provide efficient heating, low-energy neutral pions provide efficient heating at high densities, and the effectiveness of neutral pions at low densities depends on the stopping of ≈ 70 MeV photons.

We now turn to charged hadrons, which are subject to Coulomb interactions with ions and electrons as well as elastic nuclear scatters similar to their neutral brethren. At energies $\epsilon \lesssim 10$ MeV, scattering off electrons is in fact the least dominant of these processes, contrary to the behavior of terrestrial detectors. This is due to the significant Pauli-blocking of electron interactions near the Fermi energy $E_F \sim 1 - 10$ MeV. Low-energy charged hadrons will thus predominantly lose energy through elastic nuclear scatters or, within a small range of energies, Coulomb scatters off ions—either way, both length scales are well below the trigger size. In the context of a hadronic shower, the final-state hadrons are ~ 10 MeV nucleons and pions, with each species carrying an $\mathcal{O}(1)$ fraction of the initial energy. These products will thermalize within a trigger size and thus hadronic showers are an efficient heating mechanism.

b. *Electrons and Photons.* For electrons and photons below ~ 100 MeV the dominant interactions are Coulomb scatters off electrons and Compton scatters, respectively. Thus, at these energies electrons and photons rapidly thermalize in the star into a compact electromagnetic "gas" with a size set by the radiative length scale $X_{\rm EM}$. This gas cools and diffuses to larger length scales, eventually allowing subdominant processes to thermalize carbon ions. The details of this evolution depend on the initial EM gas temperature, which is set by the total SM energy released by the DM. If the gas remains above ~ 10 MeV by the time it has diffused to the photonuclear scale, photons in the gas will thermalize ions via photonuclear showers and subsequent nuclear elastic heating (see discussion above). Otherwise, electrons will thermalize ions via elastic Coulomb scatters. Note that for temperatures T less than the Fermi energy E_F, the electrons are partially degenerate and heating proceeds via the thermal tail with kinetic energies $\epsilon \sim E_F + T$. In the context of an electromagnetic shower, we expect this thermalized gas to initially have temperatures $\lesssim 100$ MeV. At these temperatures the heat capacity is dominated by photons, so as the gas diffuses to a size $\lambda_{\gamma A}$ it cools by a factor $(X_{\rm EM}/\lambda_{\gamma A})^{3/4} \sim 10^{-2} - 10^{-1}$. Therefore the relevant process to consider is the Coulomb scattering of electrons off ions, which has a stopping length

$$\lambda_{\rm coul} \approx 10^{-5} \left(\frac{\epsilon}{10 \text{ MeV}} \right) \left(\frac{10^{32} \text{ cm}^{-3}}{n_{\rm ion}} \right). \tag{12}$$

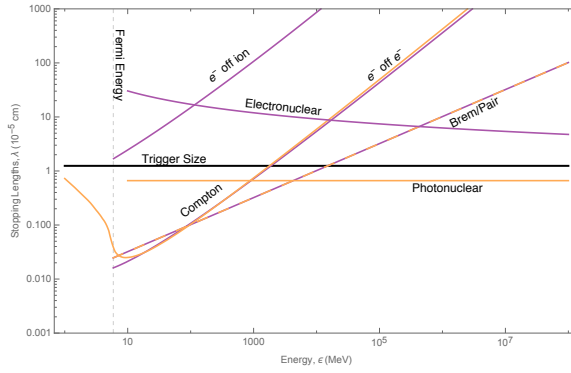As this is of order the trigger size, electromagnetic showers are also an efficient heating mechanism.

FIG. 4: Stopping lengths of incident photons and electrons as a function of kinetic energy in a WD of density update to 1.25 solar mass $n_{\rm ion} \sim 10^{32}$ cm^{-3} ($\approx 1.37~M_\odot$). Orange lines are incident photons, purple lines are incident electrons. The dashed line is the EM shower length $X_{\rm EM}$.
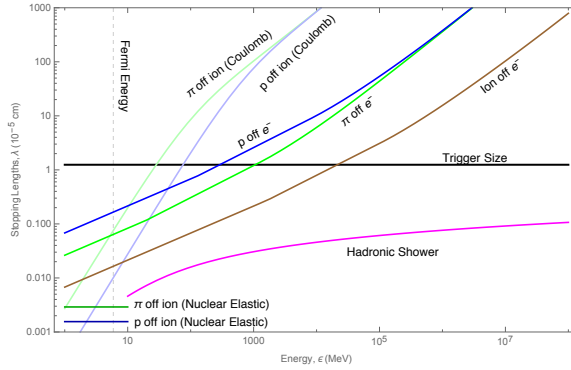

FIG. 5: Stopping lengths for incident hadrons as a function of kinetic energy in a WD of density update to 1.25 solar mass $n_{\rm ion} \sim 10^{32}$ cm^{-3} ($\approx 1.37~M_\odot$). The magenta line is the hadronic shower length $X_{\rm had}$.

IV. DARK MATTER-INDUCED IGNITION

Any DM state that produces SM particles in a WD has the potential to ignite the star, provided that sufficient SM energy is produced. The distribution in space, momentum, and species of these SM products is dependent on unknown DM physics and is needed to determine the rate of DM-induced SN. This can be done precisely for a specific DM model, as we do for Q-ball DM in Section VI. In this Section, however, we study some general features of DM-WD encounters involving DM that possesses interactions with itself and the SM. We collect below the basic formulas relating DM model parameters to ignition criteria, SN rate, etc.

DM can generically produce SM particles in the WD through three basic processes: DM-DM collisions, DM decays, and DM-SM inelastic scattering. For ultra-heavy DM, these processes can be complicated events involving many (possibly dark) final states, analogous to the interactions of heavy nuclei. We classify DM candidates into three types according to the interaction that provides the dominant source of heating, and refer to these as collision, decay, and scattering candidates. We also make the simplifying assumption that the above events are "point-like", producing SM products in a localized region (smaller than λ_T) near the interaction vertex.

The SN rate may be greatly enhanced if DM is captured in the star, so we also consider separately "transiting DM" and "captured DM". In general, there is some loss of DM kinetic energy in the WD. In the transit scenario, this energy loss is negligible and the DM simply passes through the star. In the capture scenario, the energy loss is not directly capable of ignition but is sufficient to stop the DM and cause it to accumulate in the star. Energy loss may be due to a variety of processes, but for simplicity we will focus on an elastic scattering of DM off carbon ions. Of course, due to the velocity spread of DM in the rest frame of a WD, there will necessarily be both transiting and captured DM populations in the star.

A. DM-SM Inelastic Scattering

a. Ignition Condition. Runaway fusion only occurs in the degenerate WD interior where thermal expansion is suppressed as a cooling mechanism. The outer layers of the WD, however, are composed of a non-degenerate gas and it is therefore essential that a DM candidate penetrate this layer in order to ignite a SN. We parameterize this by a DM stopping power $(dE/dx)_{\rm SP}$, the kinetic energy lost by the DM per distance traveled in the non-degenerate layer, and demand that

$$\left(\frac{dE}{dx}\right)_{\rm SP} \ll \frac{m_\chi v_{\rm esc}^2}{R_{\rm env}}, \tag{13}$$

where $R_{\rm env} \sim 50$ km is the width of a WD envelope [15].

DM-SM scattering will result in a continuous energy deposit along the DM trajectory (if the interaction is rare enough for this not to be true, then the encounter is analogous to the case of DM decay). This is best described by a linear energy transfer $(dE/dx)_{\rm LET}$, the kinetic energy of SM particles produced per distance traveled by the DM. If these products have a heating length L_0 then the energy deposit must at minimum be taken as the energy transferred along a distance L_0 of the DM trajectory. Of course, we can always choose to consider a longer segment of the trajectory. Importantly, as per the ignition condition (3), such a deposition is *less* explosive unless L_0 is smaller than the trigger size λ_T. We thus consider the energy deposited over the larger of these two length scales. Assuming the energy of the DM is roughly constant during this heating event, the ignition condition is:

$$\left(\frac{dE}{dx}\right)_{\rm LET} \gtrsim \frac{\mathcal{E}_{\rm boom}}{\lambda_T} \cdot \max\left\{\frac{L_0}{\lambda_T}, 1\right\}^2. \tag{14}$$

Note that the DM stopping power in the non-degenerate layer $(dE/dx)_{\rm SP}$ and the linear energy transfer in the degenerate interior $(dE/dx)_{\rm LET}$ are possibly controlled by different physics and may have very different numerical values. In addition, a transit event satisfying condition (13) will have negligible energy loss over the parametrically smaller distances λ_T or L_0, validating (14).

The above calculation sums the individual energy deposits along the DM trajectory as though they are all deposited simultaneously. This is valid if the DM moves sufficiently quickly so that this energy does not diffuse out of the region of interest before the DM has traversed the region. We therefore require that the diffusion time $\tau_{\rm diff}$ across a heated region of size L at temperature T_f be larger than the DM crossing-time:

$$\tau_{\rm diff} \sim \frac{L^2}{\alpha(T_f)} \gg \frac{L}{v_{\rm esc}}, \tag{15}$$

where $\alpha(T)$ is the temperature-dependent diffusivity, and the DM transits at the stellar escape velocity $v_{\rm esc} \sim 10^{-2}$. This condition is more stringent for smaller regions, so we focus on the smallest region of interest, $L = \lambda_T$. Then (15) is equivalent to demanding that the escape speed is greater than the conductive speed of the fusion wave front, $v_{\rm cond} \sim \alpha(T_f)/\lambda_T$. Numerical calculations of $v_{\rm cond}$ are tabulated in [10], and indeed condition (15) is satisfied for all WD densities.

b. Transit Scenario Event Rate. The rate of transit events is directly given by the flux of DM through a WD

$$\Gamma_{\rm trans} \sim \frac{\rho_\chi}{m_\chi} R_{\rm WD}^2 \left(\frac{v_{\rm esc}}{v_{\rm halo}}\right)^2 v_{\rm halo}, \tag{16}$$

where ρ_χ is the DM density in the region of the WD, and $R_{\rm WD}$ is the WD radius. Here $v_{\rm halo} \sim 10^{-3}$ is the virial velocity of our galactic halo. Note the $(v_{\rm esc}/v_{\rm halo})^2 \sim 100$ enhancement due to gravitational focusing.

We will not consider here captured DM heating via scattering events, as such heating will typically cause ignition before capture occurs. However, it is possible to cause ignition after capture if the capture and thermalization of DM leads to an enhanced scattering process.

B. DM-DM Collisions and DM Decays

a. Ignition Condition. For a point-like DM-DM collision or DM decay event releasing particles of heating length L_0, ignition will occur if the total energy in SM products satisfies condition (3). Such an event will likely result in both SM and dark sector products, so we parameterize the resulting energy in SM particles as a fraction $f_{\rm SM}$ of the

DM mass. For non-relativistic DM, the DM mass is the dominant source of energy and therefore $f_{\rm SM} \lesssim 1$ regardless of the interaction details. A single DM-DM collision or DM decay has an ignition condition:

$$m_\chi f_{\rm SM} \gtrsim \mathcal{E}_{\rm boom} \cdot \max\left\{\frac{L_0}{\lambda_T}, 1\right\}^3 . \tag{17}$$

We are thus sensitive to DM masses $m_\chi > 10^{15}$ GeV.

   b.   Transit Scenario Event Rate.   DM that is not captured traverses the WD in a time $t_{ff} \sim R_{\rm WD}/v_{\rm esc}$, and the rate of DM-DM collisions within the WD parameterized by cross-section $\sigma_{\chi\chi}$ is:

$$\Gamma_{\rm ann} \sim \left(\frac{\rho_\chi}{m_\chi}\right)^2 \sigma_{\chi\chi} \left(\frac{v_{\rm esc}}{v_{\rm halo}}\right)^3 v_{\rm halo} R_{\rm WD}^3 . \tag{18}$$

Similarly the net DM decay rate inside the WD parameterized by a lifetime τ_χ is:

$$\Gamma_{\rm decay} \sim \frac{1}{\tau_\chi} \frac{\rho_\chi}{m_\chi} \left(\frac{v_{\rm esc}}{v_{\rm halo}}\right) R_{\rm WD}^3 . \tag{19}$$

C.   DM Capture

   We first summarize the capture and subsequent evolution of DM in the WD, ignoring annihilations or decays. See Appendix B for details. Consider a spin-independent, elastic scattering off ions with cross section $\sigma_{\chi A}$. The rate of DM capture in gravitating bodies is of course very well-studied [18, 19]. However, this rate must be modified when the DM requires multiple scatters to lose the necessary energy for capture. Ultimately in our scenario of interest, the capture rate is of the form

$$\Gamma_{\rm cap} \sim \Gamma_{\rm trans} \cdot \min\left\{1, \overline{N}_{\rm scat} \frac{m_{\rm ion} v_{\rm esc}^2}{m_\chi v_{\rm halo}^2}\right\}, \tag{20}$$

where $\Gamma_{\rm trans}$ is the DM transit rate of Equation (16) and $\overline{N}_{\rm scat}$ is the average number of scatters during a transit:

$$\overline{N}_{\rm scat} \sim n_{\rm ion} \sigma_{\chi A} R_{\rm WD} . \tag{21}$$

The capture rate is limited by existing constraints on the DM spin-independent nucleon cross section, the most stringent of which are direction detection experiments [17]. For DM satisfying these bound, less than 1% of transiting DM is captured by the star and the capture rate in regime scales as $\Gamma_{\rm cap} \propto \frac{\sigma_{\chi A}}{m_\chi^2}$.

   Once DM is captured, it eventually thermalizes with the stellar medium and settles at to a thermal radius $R_{\rm th}$. This proceeds in two stages. Captured DM will initially be found on a large, bound orbit that decays after many transits of the WD until the orbital size is fully contained within the star. Orbit decay then continues at a faster pace, though still involving many orbits before reaching the thermal radius. The DM will begin steadily accumulating at $R_{\rm th}$, with the possibility of self-gravitational collapse if the collected mass of DM exceeds the WD mass within this volume. For DM masses $m_\chi > 10^{15}$ GeV, the thermalization timescale is dominated by the first stage and the onset of self-gravitation happens instantly relative to thermalization. Of course, not all of these stages may be reached within the age of the WD. The decay time is (see Appendix B)

$$t_1 \sim 10^{15} \text{ s} \left(\frac{m_\chi}{10^{16} \text{ GeV}}\right)^{3/2} \left(\frac{\sigma_{\chi A}}{10^{-35} \text{ cm}^2}\right)^{-3/2} \tag{22}$$

¡¡¡¡¡¡ HEAD where its kinetic energy balances against the gravitational potential energy of the (enclosed) WD mass. This thermalization time can be explicitly calculated in the case of elastic nuclear scatters [20]. First, the DM passes through the WD many times until the size of its orbit becomes fully contained within the star. This occurs after a time

$$t_1 \sim \left(\frac{m_\chi}{m_{\rm ion}}\right)^{3/2} \frac{R_{\rm WD}}{v_{\rm esc}} \frac{1}{\overline{N}_{\rm scat}} \frac{1}{\max\{\overline{N}_{\rm scat}, 1\}^{1/2}} \sim 10^{15} \text{ s} \left(\frac{m_\chi}{10^{16} \text{ GeV}}\right)^{3/2} \left(\frac{\sigma_{\chi A}}{10^{-35} \text{ cm}^2}\right)^{-3/2} . \tag{23}$$

Subsequently, the DM completes many orbits within the star until dissipation reduces the orbital size to the thermal radius. This occurs after a time

$$t_2 \sim \left(\frac{m_\chi}{m_{\rm ion}}\right) \frac{1}{n_{\rm ion} \sigma_{\chi A}} \frac{1}{v_{\rm ion}} \sim 10^{13} \text{ s} \left(\frac{m_\chi}{10^{16} \text{ GeV}}\right) \left(\frac{\sigma_{\chi A}}{10^{-35} \text{ cm}^2}\right)^{-1}, \tag{24}$$

where $v_{\rm ion} \sim \sqrt{\frac{T}{m_{\rm ion}}}$. There is an additional $\mathcal{O}(10)$ logarithmic correction in accounting for the thermalization below $v_{\rm ion}$. Note that the time to complete a single orbit is simply the gravitational free-fall timescale:

$$t_{\rm ff} \sim \sqrt{\frac{1}{G\rho_{\rm WD}}} \sim 0.1 \text{ s.} \tag{25}$$

The DM will begin steadily accumulating at $R_{\rm th}$ after a time $t_1 + t_2$. This thermalization time is dominated by t_1 at low scattering cross-sections and is less than the age of the WD for: ======= and collection progresses to collapse only if ¿¿¿¿¿¿¿ origin/master

$$\sigma_{\chi A} \gtrsim 10^{-36} \text{ cm}^2 \left(\frac{m_\chi}{10^{16} \text{ GeV}} \right). \tag{26}$$

¡¡¡¡¡¡¡ HEAD However, if the collected mass of DM at the thermal radius exceeds the WD mass within this volume, then there is the possibility of self-gravitational collapse. The time to collect a critical number of DM particles is given by

$$t_{\rm sg} \sim \frac{\rho_{\rm WD} R_{\rm th}^3}{m_\chi \Gamma_{\rm cap}} \sim 10^9 \text{ s} \left(\frac{m_\chi}{10^{16} \text{ GeV}} \right)^{-1/2} \left(\frac{\sigma_{\chi A}}{10^{35} \text{ cm}^2} \right)^{-1}. \tag{27}$$

Note that for DM masses $m_\chi > 10^{15}$ GeV, self-gravitation happens instantly relative to thermalization. Typically, the timescale for collapse is set by the DM sphere's ability to cool and shed gravitational potential energy. This is initially just t_2, while the time to collapse at any given radius r is of order

$$t_{\rm cool} \sim t_2 \min\{v_{\rm ion}/v_\chi, 1\}, \quad v_\chi \sim \sqrt{\frac{GNm_\chi}{r}}, \tag{28}$$

where N is the number of collapsing DM particles. However, since the DM collection time is shorter than the cooling time $t_{\rm sg} < t_2$, the dynamics of the collapse is initially set by further collection. This will necessarily increase the number of collapsing DM particles beyond $N \sim \Gamma_{\rm cap} t_{\rm sg}$ and hasten the collapse until the collection time matches the cooling time. ======= ¿¿¿¿¿¿¿ origin/master

At any point in this process, captured DM has the potential to ignite a SN. Of particular interest is the ability of DM to ignite the star during self-gravitational collapse, either via annihilations or the formation of a black hole. Such a process can release sufficient energy to trigger SN with DM masses less than 10^{15} GeV. However, collapsing DM involves additional subtitles that are beyond the scope of this paper, and are the focus of future work [21]. In the following we assume $m_\chi > 10^{15}$ GeV and give only a quick assessment of collapse.

We now turn to the rate of DM-DM collisions at various stages in the above evolution. The settling DM constitutes a number density throughout the WD volume and is the dominant source of annihilations for large cross-sections. The total rate of annihilations for the in-falling DM is peaked near the thermal radius

$$\Gamma_{\rm infall} \sim \frac{(\Gamma_{\rm cap} t_2)^2}{R_{\rm th}^3} \sigma_{\chi\chi} v_{\rm th}. \tag{29}$$

Where t_2 is the timescale of the second, internal thermalization stage. Only if the annihilation cross section $\sigma_{\chi\chi}$ is sufficiently small will the DM accumulate at $R_{\rm th}$ and collapse - otherwise, an in-fall annihilation ignites a SN. However, if collapse does occur, then for $m_\chi > 10^{15}$ GeV ignition is almost guaranteed if DM-DM annihilations are allowed. When the DM sphere is at a radius r, the rate of annihilations is

$$\Gamma_{\rm collapse} \sim \frac{(\rho_{\rm ion} R_{\rm th}^3 / m_\chi)^2}{r^3} \sigma_{\chi\chi} v_\chi. \tag{30}$$

¡¡¡¡¡¡¡ HEAD Here we have conservatively taken the number of collapsing particles to be the critical number—as mentioned above, this is an underestimate for such ultra-heavy DM. Of course, there may be some stabilizing pressure which prevents the DM from ever collapsing below a certain radius, similar to a black hole. To illustrate the nature of the collapse constraint, we will assume such a stable radius at which point no further annihilations take place in the "inert" DM sphere. Note that if a single collision has not occurred during collapse, one may additionally examine annihilations of the subsequent in-falling DM—for simplicity, we will not consider this scenario.

Lastly, we compute the rate of decays for captured DM. Of course, this rate is proportional to the number of DM particles in the WD available for decay at any given instance. In the wind scenario (19), this number is of order $\sim (\Gamma_{\rm trans} \times t_{\rm ff})$. In the capture scenario, this number is instead determined by the thermalization time inside the

WD: ======= Here we have conservatively taken the number of collapsing particles to be the self-gravitational threshold—as mentioned in Appendix B, this is an underestimate for ultra-heavy DM. Of course, there may be some stabilizing physics which prevents the DM from collapsing and annihilating below a certain radius, such as formation of a black hole or bound states. To illustrate the stringent nature of collapse constraint, we will assume a fiducial stable radius $R_{\rm sta}$ for PLOT. Note that if a single collision has not occurred during collapse, one may additionally examine annihilations of the subsequent in-falling DM—for simplicity, we do not consider this scenario.

Lastly, we compute the rate of decays for captured DM, which is simply proportional to the number of DM particles in the WD available for decay at any given instance. In the transit scenario (19), this number is of order $\sim (\Gamma_{\rm trans} \times t_{\rm ff})$. In the capture scenario, this number is instead determined by the second thermalization time ¿¿¿¿¿¿¿ origin/master

$$\Gamma_{\rm decay} \sim \frac{1}{\tau_\chi} \Gamma_{\rm cap} t_2 \tag{31}$$

¡¡¡¡¡¡¡ HEAD Here we have conservatively assumed that after a thermalization time, the DM quickly collapses and stabilizes to an inert state incapable of further decay. If not, the maximum possible decay rate is given by replacing $t_2 \to \tau_{\rm WD}$ in (31). ======= conservatively assuming that after a thermalization time, the DM quickly collapses and stabilizes to an inert state incapable of further decay. If this is not the case, then the maximum possible decay rate is given by replacing $t_2 \to \tau_{\rm WD}$ in the captured decay rate (31). ¿¿¿¿¿¿¿ origin/master

V. DARK MATTER CONSTRAINTS

We now constrain some simplified models of DM which will ignite a WD via one of the processes parameterized in Section IV. First, however, we review how WD observables constrain DM candidates capable of triggering SN.

A. Review of WD Observables

Following the discussion of [1], our constraints come from (1) the existence of heavy, long-lived white dwarfs, or (2) the measured type 1a SN rate. The typical age of a WD is of order the age of the universe $\sim$ Gyr. RX J0648.04418 is a nearby star and one of the heavier known WDs, with a mass $\sim 1.25\ M_\odot$ [22] and local dark matter density which we take to be $\rho_\chi \sim 0.4$ GeV/cm³. Of course, this is not the only known heavy WD—the Sloan Digital Sky Survey [23] has found 20+ others. The NuStar collaboration has also recently uncovered evidence for the likely existence of heavy WDs near the galactic center [24], where the DM density is assumed to be much greater $\rho_\chi \gtrsim 10^3$ GeV/cm³ [25]. Such heavy candidates are particularly suited for our constraints as the energy deposit necessary to trigger SN (3) is a decreasing function of WD mass. However, less dense white dwarfs are significantly more abundant in the galaxy. Thus, even if a sufficiently massive DM is unable to trigger a violent heating event within the lifetime of a WD, it could still ignite enough lighter WDs to affect the measured SN rate of ~ 0.3 per century. The DM-induced SN rate is estimated using the expected number of white dwarfs per galaxy $\sim 10^{10}$ and their mass distribution [23]. Simulations indicate that only WD masses heavier than $\sim 0.85\ M_\odot$ will result in optically visible SN [1]. Therefore, most of the stars exploded in this manner will be in the mass range $\sim 0.85 - 1\ M_\odot$, resulting in weaker SN than expected of typical Chandrasekhar mass WDs.

To summarize, a bound on DM parameters can be placed if either a single explosive event occurs during the lifetime of an observed star such as RX J0648.04418, or the SN rate due to such DM events throughout the galaxy exceeds the measured value. Note that for low-mass WDs dominated by photon diffusion, $\mathcal{E}_{\rm boom}$ is a strong function of WD density. In [1] the central WD density is used to constrain black hole transits with the justification that the density is nearly constant for much of the star. The average density for WDs is typically a factor $\sim 10^{-2} - 10^{-1}$ less than the central density, although it is found that the WD density only changes by an $\mathcal{O}(1)$ fraction from the central value up to a distance $\sim R_{\rm WD}/2$ [26]. Therefore the central density is a valid approximation as long as we consider heating events within this "modified" WD volume. For simplicity, we employ this approach.

B. Transit Constraints

In order to constrain a DM model through its transit interaction with a WD, we require that it satisfy the ignition condition (14). This is given in terms of an LET, which parameterizes the ability for DM to release sufficient energy to the star in the form of SM particles. $(dE/dx)_{\rm LET}$ for any realistic DM model would necessarily involve a sum over stellar targets along with species that could be produced, as well as an integral over the produced particle spectrum.

However, we will consider a highly simplified interaction in which $\sigma_{Ni\epsilon}$ denotes the cross-section for DM to scatter off a stellar constituent (e.g. ions), producing N particles of SM species i and individual energy ϵ. If this were the only available channel for the DM to deposit energy, then the LET could be written as

$$\left(\frac{dE}{dx}\right)_{\text{LET}} = n_{\text{ion}}\sigma_{Ni\epsilon}N\epsilon. \tag{32}$$

The heating length for such a DM-SM scattering interaction is computed in Section III.

Additionally, consider the case that the LET $(dE/dx)_{\text{LET}}$ and DM stopping power $(dE/dx)_{\text{SP}}$ are equal—that is, the DM loses kinetic energy at the same rate as energy is deposited to the WD. While such a statement is certainly not true for all DM models (such as the Q-ball, which liberates binding energy rather than transferring kinetic energy), it provides a useful benchmark to express constraints. It is interesting to note that in this case, combining the transit explosion condition (14) with (32) yields a lower bound on DM mass such that the DM is able to both penetrate the non-degenerate WD envelope *and* trigger an explosion:

$$m_\chi > \mathcal{E}_{\text{boom}}\left(\frac{R_{\text{env}}}{\lambda_T}\right)\left(\frac{\rho_{\text{env}}}{\rho_{\text{WD}}}\right)\frac{1}{v_{\text{esc}}^2}, \tag{33}$$

where ρ_{WD} is the central density of the WD. For the typical parameters of a 1.25 $M_\odot$ WD we find that the DM mass must be greater than $\sim 10^{28}$ GeV to ensure a penetrating and explosive transit, taking the density of the WD non-degenerate layer to be a nominal $\mathcal{O}(10^{-3})$ fraction of the central density [15]. In other words, if (33) were violated then the DM interaction is either not strong enough to ignite the WD or is so strong that the DM cannot penetrate the envelope without losing appreciable kinetic energy. We reiterate, however, that this bound is only applicable when the energy input to the WD is chiefly coming from the DM kinetic energy, rather than binding energy or other sources.

With the above schematic for a DM transit, we use the rates and heating lengths computed in previous sections to constrain the parameter $\sigma_{Ni\epsilon}$ as a function of DM mass m_χ. This is done in Figure 6 using the different classes of observation available and for representative choices of ϵ and SM species i released.

C. Collision and Decay Constraints

In order to constrain a DM model through its annihilations or decays within a WD, we require that it satisfy the ignition condition (17). As before, consider a simplified interaction wherein a single annihilation or decay releases N particles of SM species i and individual energy ϵ. If we assume a fractional parameter $f_{\text{SM}} = 1$, this corresponds to the entire mass of DM being converted into SM products i, each with energy m_χ/N. These will deposit their energy and thermalize ions within a distance described in Section III.

With this schematic for DM-DM collisions, we use the rates and heating lengths computed in previous sections to constrain the cross section $\sigma_{\chi\chi}$ using the different classes of observation available and for representative choices of f_{SM} and SM species i released. This is done in Figure 7 for the wind scenario and Figure **??** for the capture scenario. In the latter, we also specify a benchmark value for the DM-nuclear cross section $\sigma_{\chi A}$. Similarly, we are able to constrain the DM lifetime τ_χ in Figures 8 and **??** for the wind and capture scenarios, resepctively.

Complementary Limits It is important to note that there are additional limits on DM interactions of this kind, complementary to the limits placed from WDs. For instance, DM can annihilate or decay into ultra-high energy particles within our galactic halo and therefore contribute to the cosmic ray (CR) flux seen in terrestrial air shower detectors. As CRs of energy greater than $\sim 10^{12}$ GeV have not yet been observed [27, 28], this places a concrete limit on DM interaction parameters $\sigma_{\chi\chi}$ and τ_χ which involve the release of such ultra-high energy particles. In theory a constraint may also be placed on lower-energy SM products from DM annihilations or decays, which would provide an additional source for the measured CR flux, although such a detailed analysis is beyond the scope of this work. The CR constraint on DM can be estimated by requiring that the expected time for an event to strike earth is less than the lifetime of the detector ~ 10 yr. For a detector of area $\sim (50 \text{ km})^2$ [27], we find that the CR bounds are weaker than the WD bounds except in the DM decay "wind scenario", where the cosmic rays bounds are comparable to those due to the observation of a local WD. This coincidence is actually a consequence of the similar "space-time volumes" of the two systems. A CR detector sees events within a space-time volume $\sim (R_{\text{det}}^2 R_{\text{halo}} \times 10 \text{ yr})$ which is comparable to the WD space-time volume for decay events $\sim (R_{\text{WD}}^3 \times 10^9 \text{ yr} \times 10)$, including the $\mathcal{O}(10)$ gravitational enhancement.

In addition, there are various cosmological bounds on DM interactions. By requiring that the galactic halo has not substantially depleted during its lifetime, there is a constraint on annihilation cross section $\sigma_{\chi\chi}/m_\chi \lesssim$ barn/GeV, regardless of the precise details of the collision. This is similar in magnitude to the DM self-interaction bounds from
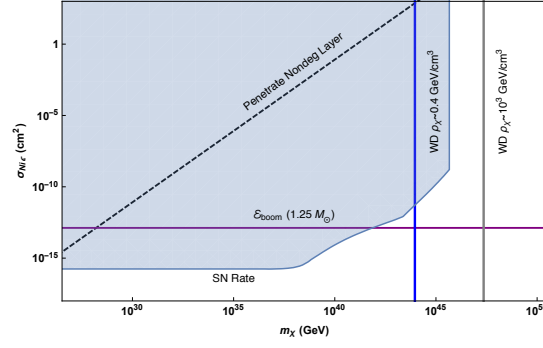
FIG. 6: Constraints on a DM-nuclei scattering cross-section to produce a single TeV photon. Bounds come from demanding that heating events satisfy (14) and occur at a rate (**??**) rapid enough to either ignite a single observed 1.25 $M_\odot$ WD in its lifetime (local and galactic center) or exceed the measured SN rate in our galaxy.

FIG. 7: Constraints on DM-DM collision cross-section into photons with individual energy $\epsilon > 10$ MeV and $f_{\rm SM} = 1$. Bounds come demanding that heating events satisfy (17) and occur at a rate (18) ("wind scenario") rapid enough to either ignite a single observed 1.25 $M_\odot$ WD in its lifetime (local and galactic center) or exceed the measured SN rate in our galaxy.
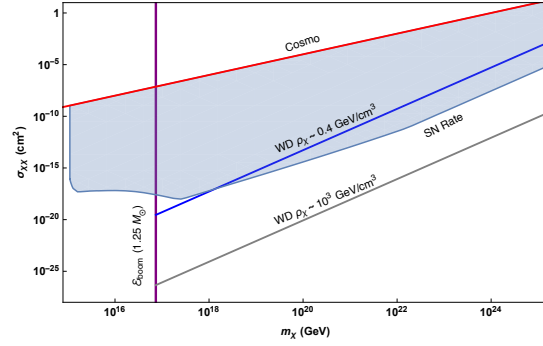
colliding galaxy clusters [29]. The cosmological bound on DM lifetime $\tau_\chi \gtrsim 100$ Gyr is also independent of the nature of the decay products (see [30] for details). Since the limits imposed by the WD scale as $\sigma_{\chi\chi} \propto m_\chi^2$ and $\tau_\chi \propto m_\chi^{-1}$, at sufficiently large DM masses these above cosmological considerations are the more stringent constraints on its interactions. This occurs for DM masses in the range $m_\chi \sim 10^{25} - 10^{30}$ GeV.
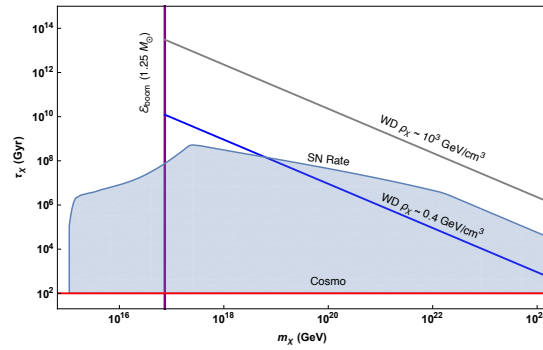

FIG. 8: Constraints on DM decay lifetime into photons with individual energy $\epsilon > 10$ MeV and $f_{\rm SM} = 1$. Bounds come demanding that heating events satisfy (17) and occur at a rate (19) ("wind scenario") rapid enough to either ignite a single observed 1.25 $M_\odot$ WD in its lifetime (local and galactic center) or exceed the measured SN rate in our galaxy.
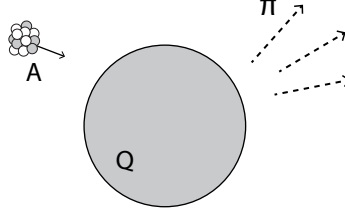
FIG. 9: Interaction of a baryonic Q-ball with a nucleus. Its constituent nucleons are destroyed as their quarks join the Q-ball condensate, with their binding energy radiated as roughly A outgoing pions of energy $\sim \Lambda_{QCD}$. The Q-ball charge increases by the nuclear baryon number A.

VI. Q-BALLS

Having derived constraints on generic models of ultra-heavy DM, we turn towards a concrete example. In various supersymmetric extensions of the SM, non-topological solitons called Q-balls can be produced in the early universe [31, 32]. If these Q-balls were stable, they would comprise a component of the DM today. For gauge-mediated models with flat scalar potentials, the Q-ball mass and radius are given by

$$M_Q \sim m_S Q^{3/4}, \quad R_Q \sim m_S^{-1} Q^{1/4}, \tag{34}$$

where m_S is related to the scale of supersymmetry breaking, and Q is the global charge of the Q-ball—in our case, baryon number. The condition $M_Q/Q < m_p$ ensures that the Q-ball is stable against decay to nucleons. When an electrically neutral baryonic Q-ball interacts with a nucleon, it absorbs its baryonic charge and induces the dissociation of the nucleon into free quarks. During this proton decay-like process, $\sim$ GeV of energy is released through the emission of 2–3 pions [33]. We assume that for each Q-ball collision, there is equal probability to produce π^0 and $\pi^{\pm}$ under the constraint of charge conservation. Note that a sufficiently massive Q-ball will become a black hole if $R_Q \lesssim G M_Q$. In the model described above, this translates into a condition $(M_{\rm pl}/m_S)^4 \lesssim Q$.

We now determine the explosiveness of a Q-ball transit. As in Section V, this process is described by the parameter

$$\left(\frac{dE}{dx}\right)_{\rm LET} \sim n_{\rm ion}\sigma_Q N\epsilon, \tag{35}$$

where the nuclear collision results in $N \sim 30$ pions released, each with kinetic energy $\epsilon \sim 500$ MeV. These pions induce hadronic showers which terminate in low-energy hadrons that rapidly transfer their energy to ions via elastic scatters, as discussed in Section III. Thus the Q-ball transit has a heating length within the trigger size, and the Q-ball cross-section necessary to ignite runaway fusion is given by equations (14) and (35):

$$\sigma_Q \gtrsim \frac{1}{n_{\rm ion}} \frac{\mathcal{E}_{\rm boom}}{\lambda_T} \left(\frac{1}{10~{\rm GeV}}\right). \tag{36}$$

We see $\sigma_Q \approx 10^{-12}$ cm^2 is sufficient to blow up a $\sim 1.25~M_\odot$ WD. The cross-section for this interaction is approximately geometric

$$\sigma_Q \sim \pi R_Q^2, \tag{37}$$

and so $Q \gtrsim 10^{42}~(m_S/{\rm TeV})^4$ can be constrained from the observation of a single, heavy WD if there is a Q-ball transit with the star's lifetime. Note that the Q-ball interaction described above results in minimal slowing or transfer of kinetic energy for Q-balls this massive, so transits will easily penetrate the non-degenerate WD envelope (13).

The existing limits on Q-balls primarily come from Super-Kamiokande and air fluorescence detectors of cosmic rays (OA, TA) [34]. However, the constraints that come from considering the ignition of WDs are in a fundamentally new and complementary region of parameter space. These are plotted in Figure 10. We have also included the constraints that result from gravitational heating of a WD during a Q-ball transit, as in [1].

VII. DISCUSSION

The detection of ultra-heavy DM is an open problem which will likely require a confluence of astrophysical probes. Here we present a guide to containing these DM candidates through annihilations, decays, and transits inside a WD
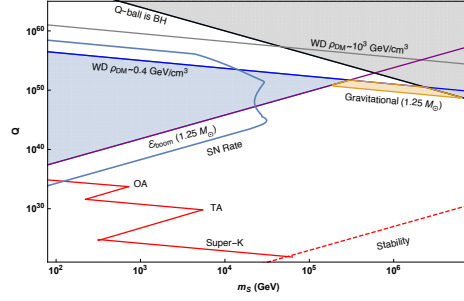
FIG. 10: Constraints on baryonic Q-balls that transit a WD and heat the star via strong interactions with ions. Also shown are the constraints from gravitational heating of WDs (orange), and the existing limits from terrestrial detectors (red) [34]

that release sufficient SM energy to trigger a type 1a supernova. In particular, we calculate the energy loss of high-energy particles due to SM interactions within the WD medium and determine the conditions for which a general energy deposition will heat a WD and ignite runaway fusion. The formalism provided will enable WDs to be applied as detectors for any DM models capable of heating the star through non-gravitational interactions.

In general, the phenomenology of such a DM-induced event will be the ignition of sub-Chandrasekhar mass progenitors. This raises the tantalizing possibility that DM encounters with a WD can act as an alternative explosion mechanism and progenitor system for type 1a SN. For decades, it has been widely regarded that type 1a SN are caused by accretion onto carbon-oxygen white dwarfs in binary systems that reach the critical $\approx 1.4\ M_\odot$ Chandrasekhar mass limit. Nevertheless, it is well-known that such a mechanism cannot account for all observed type 1a SN. Recent observations [5, 6] suggest that an $\mathcal{O}(1)$ fraction of the observed type 1a SN appear to have sub-Chandrasekhar progenitors. A leading explanation for this phenomenon is the detonation of a surface layer of helium which drives a shock into the interior of a sub-Chandrasekhar-mass WD [7, 8]. Another possibility is the binary merger of WDs [9]. However, in light of the lack of understanding of DM and its interactions, it is worthwhile to consider whether DM encounters with WDs may also give rise to type 1a SN progenitor.

A. PARTICLE STOPPING IN A WHITE DWARF

Here we provide a more detailed analysis of the stopping power (energy loss per distance traveled) of high-energy SM particles in a carbon-oxygen WD due to strong and electromagnetic interactions. We consider incident electrons, photons, pions, and nucleons with kinetic energy greater than an MeV.

A. WD Medium

For the WD masses that we consider, the stellar medium consists of electrons and fully-ionized carbon nuclei with densities in the range $n_e = Z n_{\rm ion} \sim 10^{31} - 10^{33}$ cm^{-3} where $Z = 6$. The internal temperature is $T \sim$ keV [15]. The electrons are a degenerate and predominantly relativistic free gas, with Fermi energy

$$E_F \sim (3\pi^2 n_e)^{1/3} \sim 1 - 10 \text{ MeV}. \tag{38}$$

The carbon ions, however, are non-degenerate and do not form a free gas. The plasma frequency due to ion-ion Coulomb interactions is given by

$$\Omega_p = \left(\frac{4\pi n_{\rm ion} Z^2 \alpha}{m_{\rm ion}} \right)^{1/2} \sim 1 - 10 \text{ keV}, \tag{39}$$

where $m_{\rm ion}$ is the ion mass. Finally, the medium also contains thermal photons, though these are never significant for stopping particles as the photon number density $n_\gamma \sim T^3$ is much smaller than that of electrons or ions.

B. Nuclear Interactions

a. Elastic Scattering of Hadrons. Hadrons with energy less than the nuclear binding energy $E_{\rm nuc} \sim 10$ MeV will predominantly stop due to elastic nuclear scatters with ions. These are hard scatters, resulting in a stopping power

$$\frac{dE}{dx} \sim n_{\rm ion}\sigma_{\rm el}\left(\frac{m}{m_{\rm ion}}\right)E \tag{40}$$

for a hadron of mass $m \ll m_{\rm ion}$ and kinetic energy E. $\sigma_{\rm el}$ is the elastic nuclear scattering cross-section, which is of order $\sigma_{\rm el} \approx$ b at these energies and drops to $\sigma_{\rm el} \approx 0.1$ b above 10 MeV [35], ignoring the nontrivial effect of nuclear resonances in the intermediate regime $1 - 10$ MeV.

b. Inelastic Scattering of Hadrons. For energies above $E_{\rm nuc}$, the stopping of hadrons is dominated by inelastic nuclear scatters. In such a collision, an incoming hadron interacts with one or more nucleons to produce a $\mathcal{O}(1)$ number of additional hadrons which approximately split the initial energy. At incident energy greater than $\sim$ GeV, the majority of secondary hadrons are pions with transverse momenta ~ 100 MeV [35]. Below $\sim$ GeV, it is found that roughly equal fractions of protons, neutrons, and pions are produced in each collision [36]. We will thus have a roughly collinear shower terminating at an energy ~ 10 MeV which consists of pions for most of the shower's development and converts to an mix of pions and nucleons in the final decade of energy. This cascade is described by a radiative stopping power

$$\frac{dE}{dx} \sim n_{\rm ion}\sigma_{\rm inel}E, \tag{41}$$

where the inelastic nuclear cross-section is given by $\sigma_{\rm inel} \approx 100$ mb and roughly constant in energy [35]. The total length of the shower is only logarithmically dependent on the initial hadron energy E,

$$X_{\rm had} \sim \frac{1}{n_{\rm ion}\sigma_{\rm inel}}\log\left(\frac{E}{E_{\rm nuc}}\right). \tag{42}$$

c. Photonuclear Interactions. Photons of energy greater than 10 MeV can also strongly interact with nuclei through the production of virtual quark-antiquark pairs. This is the dominant mode of photon energy loss at high energy. The photonuclear scatter destroys the photon and fragments the nucleus, producing secondary hadrons in a shower analogous to that described above. The photonuclear cross-section $\sigma_{\gamma A}$ is roughly given by $\sigma_{\gamma A} \approx \alpha\sigma_{\rm inel}$, again ignoring the nuclear resonances that occur for $E \lesssim$ GeV. [35] For $E \gtrsim$ GeV, $\sigma_{\gamma A}$ is likely a slowly increasing function of energy due to the coherent interaction of the photon over multiple nucleons [37], however, instead of extrapolating this behavior we conservatively take a constant photonuclear cross-section $\sigma_{\gamma A} \approx 1$ mb.

d. Electronucelar Interactions. Electrons can similarly lose energy to nuclei by radiating a virtual photon that undergoes a photonuclear scatter, which indeed provides the dominant energy loss for high energy electrons. The cross-section for this process is roughly given by the photonuclear cross-section, scaled by a factor representing the probability to radiate such a photon. This can be estimated with the Weizsacker-Williams approximation, which gives a stopping power that is suppressed from the photonuclear result by α but enhanced by an $\mathcal{O}(10)$ logarithmic phase space factor [37]:

$$\frac{dE}{dx} \sim \alpha n_{\rm ion}\sigma_{\gamma A}E\log\left(\frac{E}{m_e}\right). \tag{43}$$

Unlike the photonuclear interaction, the electronuclear event is a radiative process that preserves the original electron while leaving hadronic showers in its wake.

C. Radiative Processes

Electromagnetic showers due to successive bremsstrahlung and pair production events off carbon ions are the dominant stopping mechanisms for intermediate-energy electrons and photons. Both of these processes result in radiative stopping powers, derived semi-classically as [38]

$$\frac{dE}{dx} \sim \frac{E}{X_0}, \quad X_0^{-1} = 4n_{\rm ion}Z^2\frac{\alpha^3}{m_e^2}\log\Lambda. \tag{44}$$

X_0 is the well-known radiation length, and $\log\Lambda$ is a Coulomb form factor given by the range of effective impact parameters b:

$$\Lambda = \frac{b_{\max}}{b_{\min}}. \tag{45}$$

The maximal impact parameter is set by the plasma screening length (see A D 0 a) and the minimum by the electron mass, below which the semi-classical description breaks down. Note that for the highest WD densities $\Lambda \lesssim 1$, in which case (44) ought be replaced by a fully quantum mechanical result as in [39]. This still results in a radiative stopping power, and so for simplicity we employ (44) with $\log\Lambda \sim \mathcal{O}(1)$ for all WD densities.

a. LPM Suppression A radiative event involving momentum transfer q to an ion must, quantum mechanically, occur over a length $\sim q^{-1}$. All ions within this region contribute to the scattering of the incident particle, and for sufficiently small q this results in a decoherence that suppresses the formation of photons or electron-position pairs. This is the "Landau-Pomeranchuk-Midgal" (LPM) effect. The momentum transfer q in a given event decreases with increasing incident particle energy, and so the LPM effect will suppress radiative processes for energies greater than some scale E_{LPM}. This can be calculated semi-classically [38],

$$E_{\mathrm{LPM}} = \frac{m_e^2 X_0 \alpha}{4\pi} \approx 1 \text{ MeV} \left(\frac{10^{32}\mathrm{cm}^{-3}}{n_{\mathrm{ion}}} \right). \tag{46}$$

which is quite small due to the high ion density in the WD. The stopping power for bremsstrahlung and pair production in the regime of LPM suppression $E > E_{\mathrm{LPM}}$ is

$$\frac{dE}{dx} \sim \frac{E}{X_0} \left(\frac{E_{\mathrm{LPM}}}{E} \right)^{1/2} \quad E > E_{\mathrm{LPM}}. \tag{47}$$

In addition to the LPM effect, soft bremsstrahlung may be suppressed in a medium as the emitted photon acquires an effective mass of order the plasma frequency Ω_p. However, for high-energy electrons this dielectric suppression only introduces a minor correction to (47), in which soft radiation is already suppressed [38].

D. Elastic EM Scattering

a. Coulomb Scattering off Ions. Coulomb collisions with ions are the mechanism by which electrons of energy $1 - 10$ MeV ultimately thermalize ions. In this scenario we may treat the ions as stationary and ignore their recoil during collisions. The nuclear charge will be screened by the mobile electrons of the medium, so incident particles scatter via a potential

$$V(\mathbf{r}) = \frac{Z\alpha}{r} e^{-\lambda_{\mathrm{TF}} r}. \tag{48}$$

The screening length λ_{TF} is given in the Thomas-Fermi approximation by [40]:

$$\lambda_{\mathrm{TF}}^2 = \frac{E_F}{6\pi\alpha n_e} \sim \frac{1}{\alpha n_e^{2/3}} \tag{49}$$

where E_F is the electron Fermi energy. This plasma screening suppresses scatters with momentum transfers below $\sim \lambda_{\mathrm{TF}}^{-1}$, corresponding to a minimal energy transfer of $\omega_{\min} = \lambda_{\mathrm{TF}}^{-2}/2m_{\mathrm{ion}}$. Ions may in principle also cause screening through lattice distortion, however this may be ignored as the sound speed of the lattice $c_s \sim 10^{-2}$ is much smaller than the speed of an incident relativistic electron. Using the Born approximation, we have a cross-section for energy transfer ω

$$\frac{d\sigma}{d\omega} = \frac{2\pi Z^2 \alpha^2}{m_{\mathrm{ion}} v^2} \frac{1}{(\omega + \omega_{\min})^2} \tag{50}$$

and a stopping power

$$\frac{dE}{dx} = \int_0^{\omega_{\max}} d\omega \, n_{\mathrm{ion}} \frac{d\sigma}{d\omega} \omega \approx \frac{2\pi \, n_{\mathrm{ion}} Z^2 \alpha^2}{m_{\mathrm{ion}} v^2} \log\left(\frac{\omega_{\max}}{\omega_{\min}} \right) \tag{51}$$

where the second line is valid if $\omega_{\max} \gg \omega_{\min}$. $\omega_{\max}$ is the maximum possible energy transfer. This may be due to 4-momentum conservation, or in the case of incident electrons, the impossibility of scattering to a final energy less than E_F. 4-momentum conservation sets an upper bound ω_{kin}, which for a stationary target is

$$\omega_{\mathrm{kin}} = \frac{2 m_{\mathrm{ion}} p^2}{m_{\mathrm{ion}}^2 + m^2 + 2E m_{\mathrm{ion}}} \tag{52}$$

with p, E the incoming momentum and energy. The Fermi upper bound is simply $\omega_F = E - E_F$ so for incident electrons we take $\omega_{\max} = \min(\omega_{\mathrm{kin}}, \omega_F)$.

For scatters that transfer energy less than the plasma frequency Ω_p, one may be concerned about phonon excitations. We estimate this by treating each ion as an independent oscillator with frequency Ω_p (an Einstein solid) and compute the stopping power due to scatters which excite a single oscillator quanta. There are two key differences between this and the free ion case: incident particles must transfer an energy Ω_p and the cross-section to transfer momentum q is suppressed by a factor $q^2 / 2 m_{\mathrm{ion}} \Omega_p = \omega_{\mathrm{free}}/\Omega_p$. ω_{free} is the energy transfer that would accompany a free ion scatter with momentum transfer q. The resulting stopping power is unchanged from the free case (51), as the increased energy transfer compensates for the suppressed cross-section:

$$d\sigma \cdot \omega \sim d\sigma_{\mathrm{free}} \frac{\omega_{\mathrm{free}}}{\Omega_p} \cdot \Omega_p \sim d\sigma_{\mathrm{free}} \cdot \omega_{\mathrm{free}}. \tag{53}$$

Finally, we note that for highly energetic incident particles the cross-section (50) should be modified to account for the recoil of the ion. However, at such energies the dominant stopping power will be from hadronic or electromagnetic showers anyway.

   b. Coulomb Scattering off Electrons. The scattering of incident electrons off degenerate electrons determines the termination energy of electromagnetic showers. This calculation demands two considerations not present when scattering off ions: the targets are not stationary and they require a threshold energy transfer in order to be scattered out of the Fermi sea. However in the regime of interest $E \gg E_F$, the electron stopping power off electrons is ultimately of the same form as the stopping power off ions (51). For incident momenta much greater than the Fermi momentum, the relative velocity is of order the incident velocity and the deflection of the incident particle will generally be small. It is reasonable then that scattering proceeds, up to $\mathcal{O}(1)$ factors, as though a heavy incident particle is striking a light, stationary target. The cross-section is then given by the usual result,

$$\frac{d\sigma}{d\omega} \approx \frac{2\pi\alpha^2}{E_F} \frac{1}{\omega^2}, \tag{54}$$

where we have accounted for the target's motion by replacing its mass with its relativistic inertia $\approx E_F$. Note that plasma screening can be ignored, as Pauli-blocking will provide a more stringent cutoff on soft scatters in this case. Scatters which transfer an energy $\omega \leq E_F$ will have a suppressed contribution to the stopping power as they can only access a fraction of the Fermi sea. For incident energies $E \gg E_F$ it is sufficient to ignore these suppressed scatters:

$$\begin{aligned}
\frac{dE}{dx} &= \int_{E_F}^{\omega_{\max}} d\omega \, n_e \frac{d\sigma}{d\omega} \omega \\
&\approx \frac{2\pi \, n_e \alpha^2}{E_F} \log\left(\frac{\omega_{\max}}{E_F}\right)
\end{aligned} \tag{55}$$

where, as described above, $\omega_{\max} = \min(\omega_{\mathrm{kin}}, \omega_F)$. This derivation is admittedly quite heuristic, and so it has been checked with a detailed numerical calculation accounting fully for the target's motion and degeneracy. Equation (55) is indeed a good approximation to the stopping power for incident energies larger than the Fermi energy.

   c. Compton Scattering Compton scattering off degenerate electrons is the dominant interaction for photons of incident energy $k \leq E_F$. As we will show, this stopping power is parametrically different from that of high-energy photons due to Pauli-blocking and the motion of the electron. For $k > E_F$, the effect of Pauli-blocking is negligible and the stopping power is simply:

$$\frac{dk}{dx} \sim \frac{\pi\alpha^2 n_e}{E_F} \log\left(\frac{k}{E_F}\right), \tag{56}$$

boosting the usual result for stationary electrons. We now turn to the regime of interest, $k < E_F$. Only those electrons near the top of the Fermi sea are available to scatter, so the photon interacts with an effective electron density of

$$n_{\mathrm{eff}} = \int_{E_F - k}^{E_F} g(E) \, dE \approx 3 n_e \frac{k}{E_f} \tag{57}$$

where $g(E)$ is the Fermi density of states. In addition, Compton scatters will only occur off electrons moving roughly collinear with the photon momentum - a head-on collision would result in an energy loss for the electron, which is forbidden by Pauli exclusion. In the electron rest frame these collinear scatters are Thompson-like, and the photon energy loss is dominated by backward scatters. For relativistic electrons near the Fermi surface, these scatters transfer an energy

$$\omega \sim k \left(1 - \frac{m_e^2}{4E_F^2}\right) \approx k. \tag{58}$$

The cross section can be taken in the electron rest frame $\sigma_T \sim \alpha^2/m_e^2$, along with an 'aiming' factor $1/4\pi$ to account for the restriction to initially parallel trajectories. This gives a stopping power

$$\frac{dk}{dx} \approx \frac{\alpha^2 n_e k^2}{m_e^2 E_F}. \tag{59}$$

B. DARK MATTER CAPTURE

Here we give a more detailed discussion of DM capture and thermalization.

A. Capture Rate

For the DM to ultimately be captured, it must lose energy $\sim m_\chi v^2$, where v is the DM velocity (in the rest frame of the WD) asymptotically far away. Since typically $v \ll v_{\rm esc}$, the DM has velocity $v_{\rm esc}$ while in the star and must lose a fraction $(v/v_{\rm esc})^2$ of its kinetic energy to become captured. Properly, the DM velocity is described by a boosted Maxwell distribution peaked at the galactic virial velocity $v_{\rm halo} \sim 10^{-3}$. However, this differs from the ordinary Maxwell distribution by only $\mathcal{O}(1)$ factors [19], and we can approximate it by (ignoring the exponential Boltzmann tail):

$$\frac{dn_\chi}{dv} \approx \begin{cases} \frac{\rho_\chi}{m_\chi}\left(\frac{v^2}{v_{\rm halo}^3}\right) & v \leq v_{\rm halo} \\ 0 & v > v_{\rm halo} \end{cases}. \tag{60}$$

The DM capture rate is given by an integral of the DM transit rate weighted by a probability for capture $P_{\rm cap}$

$$\Gamma_{\rm cap} \sim \int dv \frac{d\Gamma_{\rm trans}}{dv} P_{\rm cap}(v), \tag{61}$$

where the (differential) transit rate is

$$\frac{d\Gamma_{\rm trans}}{dv} \sim \frac{dn_\chi}{dv} R_{\rm WD}^2 \left(\frac{v_{\rm esc}}{v}\right)^2 v. \tag{62}$$

$P_{\rm cap}$ depends on both the *average* number of scatters in a WD

$$\overline{N}_{\rm scat} \sim n_{\rm ion}\sigma_{\chi A} R_{\rm WD}, \tag{63}$$

and the number of scatters *needed* for capture

$$N_{\rm cap} \sim \max\left\{1, \frac{m_\chi v^2}{m_{\rm ion} v_{\rm esc}^2}\right\}, \tag{64}$$

and is most generally expressed as a Poisson sum

$$P_{\rm cap} = 1 - \sum_{n=0}^{N_{\rm cap}-1} \exp(-\overline{N}_{\rm scat})\frac{(\overline{N}_{\rm scat})^n}{n!}. \tag{65}$$

For our purposes we will approximate the sum as follows:

$$P_{\rm cap} \approx \begin{cases} 1 & \overline{N}_{\rm scat} > N_{\rm cap} \\ \overline{N}_{\rm scat} & \overline{N}_{\rm scat} < N_{\rm cap} \text{ and } N_{\rm cap} = 1 \\ 0 & \text{else} \end{cases}. \tag{66}$$

Here we ignore the possibly of capture if $\overline{N}_{\text{scat}} < N_{\text{cap}}$ except in the special case that only one scatter is needed for capture. If $\overline{N}_{\text{scat}} > N_{\text{cap}}$, we assume all DM is captured. Most accurately, this capture rate should be computed numerically, e.g. see [41] for a detailed calculation. However with the above simplifications we find that the capture rate is of order

$$\Gamma_{\text{cap}} \sim \Gamma_{\text{trans}} \cdot \min\left\{1, \overline{N}_{\text{scat}}\min\{B,1\}\right\}, \tag{67}$$
$$B \equiv \frac{m_{\text{ion}}v_{\text{esc}}^2}{m_\chi v_{\text{halo}}^2}.$$

B here encodes the necessity of multiple scattering for capture. For ultra-heavy DM $m_\chi > 10^{15}$ GeV, $B \ll 1$ and multiple scatters are always needed.

B.   Thermalization and Collapse

We consider energy loss via spin-independent, elastic scattering of DM off ions with cross section $\sigma_{\chi A}$. For the remainder of this section all numerical quantities are evaluated at a WD density $n_{\text{ion}} \sim 10^{31}$ cm^{-3}, for which the relevant WD parameters are [12]:

$$M_{\text{WD}} \sim 1.25\ M_\odot$$
$$R_{\text{WD}} \sim 4000\ \text{km}$$
$$v_{\text{esc}} \sim 2 \times 10^{-2}. \tag{68}$$

We also assume a typical WD temperature $T \sim$ keV.

To compare with existing constraints, we relate $\sigma_{\chi A}$ to the per-nucleon cross section.

$$\sigma_{\chi A} = A^2 \left(\frac{\mu_{\chi A}}{\mu_{\chi n}}\right)^2 F^2(q)\sigma_{\chi n} \sim A^4 F^2(q)\sigma_{\chi n}, \tag{69}$$

where $F^2(q)$ is the Helm form factor [16]. For DM at the WD escape velocity, the typical momentum transfer to ions is $q \sim \mu_{\chi A}v_{\text{esc}} \sim 200$ MeV and the energy transfer is $\omega \sim q^2/m_{\text{ion}} \sim$ MeV. As this q is less than or of order the inverse nuclear size, DM scattering off nuclei will be coherently enhanced. We find $F^2(q) \approx 0.1$ for $q \sim 200$ MeV. It follows that for any DM candidate satisfying the direct detection constraint (??), only a small fraction of transiting DM is captured by the star.

Once DM is captured, it thermalizes to an average velocity

$$v_{\text{th}} \sim \sqrt{\frac{T}{m_\chi}} \sim 10^{-12} \left(\frac{m_\chi}{10^{16}\ \text{GeV}}\right)^{-1/2} \tag{70}$$

and settles to the thermal radius

$$R_{\text{th}} \sim \left(\frac{T}{Gm_\chi\rho_{\text{WD}}}\right)^{1/2} \sim 0.1\ \text{cm} \left(\frac{m_\chi}{10^{16}\ \text{GeV}}\right)^{-1/2}, \tag{71}$$

where its kinetic energy balances against the gravitational potential energy of the (enclosed) WD mass. This thermalization time can be explicitly calculated for elastic nuclear scatters [20]. First, the DM passes through the WD many times until the size of its orbit becomes fully contained within the star. This occurs after a time

$$t_1 \sim \left(\frac{m_\chi}{m_{\text{ion}}}\right)^{3/2} \frac{R_{\text{WD}}}{v_{\text{esc}}} \frac{1}{\overline{N}_{\text{scat}}} \frac{1}{\max\{\overline{N}_{\text{scat}},1\}^{1/2}} \sim 10^{15}\ \text{s} \left(\frac{m_\chi}{10^{16}\ \text{GeV}}\right)^{3/2} \left(\frac{\sigma_{\chi A}}{10^{-35}\ \text{cm}^2}\right)^{-3/2}. \tag{72}$$

Subsequently, the DM completes many orbits within the star until dissipation reduces the orbital size to the thermal radius. This occurs after a time

$$t_2 \approx \left(\frac{m_\chi}{m_{\text{ion}}}\right) \frac{1}{n_{\text{ion}}\sigma_{\chi A}} \frac{1}{v_{\text{ion}}} \sim 10^{13}\ \text{s} \left(\frac{m_\chi}{10^{16}\ \text{GeV}}\right) \left(\frac{\sigma_{\chi A}}{10^{-35}\ \text{cm}^2}\right)^{-1}, \tag{73}$$

where $v_{\rm ion} \sim \sqrt{\frac{T}{m_{\rm ion}}}$. Note that the time to complete a single orbit is simply the gravitational free-fall timescale:

$$t_{\rm ff} \sim \sqrt{\frac{1}{G\rho_{\rm WD}}} \sim 0.1 \text{ s.} \tag{74}$$

The DM will begin steadily accumulating at $R_{\rm th}$ after a time $t_1 + t_2$. This thermalization time is dominated by t_1 at low scattering cross-sections and is less than the age of the WD for:

$$\sigma_{\chi A} \gtrsim 10^{-36} \text{ cm}^2 \left(\frac{m_\chi}{10^{16} \text{ GeV}}\right). \tag{75}$$

However, if the collected mass of DM at the thermal radius exceeds the WD mass within this volume, then there is the possibility of self-gravitational collapse. The time to collect a critical number of DM particles is given by

$$t_{\rm sg} \sim \frac{\rho_{\rm WD} R_{\rm th}^3}{m_\chi \Gamma_{\rm cap}} \sim 10^9 \text{ s} \left(\frac{m_\chi}{10^{16} \text{ GeV}}\right)^{-1/2} \left(\frac{\sigma_{\chi A}}{10^{35} \text{ cm}^2}\right)^{-1}. \tag{76}$$

Note that for DM masses $m_\chi > 10^{15}$ GeV, self-gravitation happens instantly relative to thermalization. Typically, the timescale for collapse is set by the DM sphere's ability to cool and shed gravitational potential energy. This is initially just t_2, while the time to collapse at any given radius r is of order

$$t_{\rm cool} \sim t_2 \min\{v_{\rm ion}/v_\chi, 1\}, \quad v_\chi \sim \sqrt{\frac{GNm_\chi}{r}}, \tag{77}$$

where N is the number of collapsing DM particles. However, since the DM collection time is shorter than the cooling time $t_{\rm sg} < t_2$, the dynamics of the collapse is initially set by further collection. This over-collection will necessarily increase the number of collapsing DM particles and hasten the collapse until the collection time matches the cooling time.

Acknowledgements

---

[1] P. W. Graham, S. Rajendran and J. Varela, Phys. Rev. D **92**, no. 6, 063007 (2015) [arXiv:1505.04444 [hep-ph]].
[2] D. S. Akerib *et al.* [LUX Collaboration], Phys. Rev. Lett. **118**, no. 2, 021303 (2017) [arXiv:1608.07648 [astro-ph.CO]].
[3] R. Agnese *et al.* [SuperCDMS Collaboration], Phys. Rev. Lett. **120**, no. 6, 061802 (2018) [arXiv:1708.08869 [hep-ex]].
[4] K. Griest, A. M. Cieplak and M. J. Lehner, Astrophys. J. **786**, no. 2, 158 (2014) [arXiv:1307.5798 [astro-ph.CO]].
[5] R. Scalzo *et al.* [Nearby Supernova Factory Collaboration], Mon. Not. Roy. Astron. Soc. **440**, no. 2, 1498 (2014) [arXiv:1402.6842 [astro-ph.CO]].
[6] R. A. Scalzo, A. J. Ruiter and S. A. Sim, Mon. Not. Roy. Astron. Soc. **445**, no. 3, 2535 (2014) [arXiv:1408.6601 [astro-ph.HE]].
[7] S. E. Woosley and T. A. Weaver, Astrophysical Journal **423**, pp.371-379 (1994).
[8] M. Fink, W. Hillebrandt and F. K. Roepke, Astron. Astrophys. [Astron. Astrophys. **476**, 1133 (2007)] [arXiv:0710.5486 [astro-ph]].
[9] R. Pakmor, M. Kromer and S. Taubenberger, Astrophys. J. **770**, L8 (2013) [arXiv:1302.2913 [astro-ph.HE]].
[10] F. X. Timmes and S. E. Woosley, Astro. Phys. Journal **396**, 649 (1992).
[11] L. R. Gasques, A. V. Afanasjev, E. F. Aguilera, M. Beard, L. C. Chamon, P. Ring, M. Wiescher and D. G. Yakovlev, Phys. Rev. C **72**, 025806 (2005) [astro-ph/0506386].
[12] F. X. Timmes, link
[13] R. Gandhi, C. Quigg, M. H. Reno and I. Sarcevic, Phys. Rev. D **58**, 093009 (1998) [hep-ph/9807264].
[14] J. A. Formaggio and G. P. Zeller, Rev. Mod. Phys. **84**, 1307 (2012) [arXiv:1305.7513 [hep-ex]].
[15] R. Kippenhahn and A. Weigert, "Stellar Structure and Evolution, Springer (1994).
[16] R. H. Helm, Phys. Rev. **104**, 1466 (1956).
[17] E. Aprile *et al.* [XENON Collaboration], Phys. Rev. Lett. **119**, no. 18, 181301 (2017) [arXiv:1705.06655 [astro-ph.CO]].
[18] W. H. Press and D. N. Spergel, Astrophys. J. **296**, 679 (1985).
[19] A. Gould, Astrophys. J. **321**, 571 (1987).

[20] C. Kouvaris and P. Tinyakov, Phys. Rev. D **83**, 083512 (2011) [arXiv:1012.2039 [astro-ph.HE]].

[21] R. Janish, V. Narayan, and P. Riggins, in preparation

[22] S. Mereghetti, arXiv:1302.4634 [astro-ph.HE].

[23] S. J. Kleinman, S. O. Kepler, D. Koester, I. Pelisoli *et al.*, Astrophys. J. Suppl. **204**, article id. 5, 14 pp. (2013)

[24] K. Perez, C. J. Hailey, F. E. Bauer, *et al.*, Nature **520**, 646 (2015)

[25] F. Nesti and P. Salucci, JCAP **1307**, 016 (2013) [arXiv:1304.5127 [astro-ph.GA]].

[26] S. Chandrasekhar, "An Introduction to the Study of Stellar Structure", University of Chicago press (1939).

[27] A. Aab *et al.* [Pierre Auger Collaboration], JCAP **1508**, 049 (2015) [arXiv:1503.07786 [astro-ph.HE]].

[28] T. Abu-Zayyad *et al.* [Telescope Array Collaboration], Astrophys. J. **768**, L1 (2013) [arXiv:1205.5067 [astro-ph.HE]].

[29] S. W. Randall, M. Markevitch, D. Clowe, A. H. Gonzalez and M. Bradac, Astrophys. J. **679**, 1173 (2008) [arXiv:0704.0261 [astro-ph]].

[30] V. Poulin, P. D. Serpico and J. Lesgourgues, JCAP **1608**, no. 08, 036 (2016) [arXiv:1606.02073 [astro-ph.CO]].

[31] S. R. Coleman, Nucl. Phys. B **262**, 263 (1985) Erratum: [Nucl. Phys. B **269**, 744 (1986)].

[32] A. Kusenko and M. E. Shaposhnikov, Phys. Lett. B **418**, 46 (1998) [hep-ph/9709492].

[33] A. Kusenko, V. Kuzmin, M. Shaposhnikov, P. G. Tinyakov, Phys. Rev. Lett. **80**, 15 (1998) [hep-ph//9712212].

[34] M. Dine and A. Kusenko, Rev. Mod. Phys. **76**, 1 (2003) [hep-ph/0303065].

[35] S. Tavernier, "Experimental Techniques in Nuclear and Particle Physics", Springer (2010).

[36] T. S. H. Lee and R. P. Redwine, Annu. Rev. Nucl. Part. Sci **52**, pp.23-63 (2002)

[37] L. Gerhardt and S. R. Klein, Phys. Rev. D **82**, 074017 (2010) [arXiv:1007.0039 [hep-ph]].

[38] S. Klein, Rev. Mod. Phys. **71**, 1501 (1999) [hep-ph/9802442].

[39] H. Bethe and W. Heitler Proc. R. Soc. Lond. A 1934 146 83-112

[40] S. L. Shapiro and S. A. Teukolsky, "Black Holes, White Dwarfs, and Neutron Stars", Wiley (1983).

[41] J. Bramante, A. Delgado and A. Martin, Phys. Rev. D **96**, no. 6, 063002 (2017) [arXiv:1703.04043 [hep-ph]].

[42] B. Rossi, "High Energy Particles", Prentice-Hall, Inc., Englewood Cliffs, NJ (1952).

[43] J. D. Jackson, "Classical Electrodynamics", 3rd edition, John Wiley and Sons, New York, (1998).